

Mechanical losses and stability performance of NEXCERA in ultra-stable laser cavities

Nico Wagner,^{1,2,*} Mateusz Narożnik,^{3,*} Marcin Bober,³ Steffen Sauer,^{1,2} Michał Zawada,³ and Stefanie Kroker^{1,2,4}

¹*Institut für Halbleitertechnik, Technische Universität Braunschweig,
Hans-Sommer-Str. 66, Braunschweig, 38106 Germany*

²*Laboratory for Emerging Nanometrology, Langer Kamp 6a-b, Braunschweig, 38106 Germany*

³*Institute of Physics, Faculty of Physics, Astronomy and Informatics,*

Nicolaus Copernicus University, Grudziądzka 5, PL-87-100 Toruń, Poland

⁴*Physikalisch-Technische Bundesanstalt, Bundesallee 100, 38116 Braunschweig, Germany*

(Dated: September 24, 2024)

NEXCERA has been recently introduced as novel ceramic-based material for spacers of ultra-stable laser cavities with a zero-crossing coefficient of thermal expansion at room temperature. Brownian thermal noise currently limits the performance of these cavities, and the mechanical loss factor, a critical parameter in estimating this noise, remains unknown for NEXCERA. In this work, we investigate the mechanical loss factor of NEXCERA N117B at room temperature across different resonance frequencies using the Gentle Nodal Suspension technique. We measure a promising loss factor of $\phi = 1.89 \times 10^{-5}$, indicating NEXCERA's potential for ultra-stable laser cavities. Based on these results, we calculate the thermal noise when NEXCERA is used as a spacer and compare its overall performance as a spacer material to widely used materials such as ULE and Zerodur, considering various substrate materials. Our findings suggest that NEXCERA is a strong candidate due to its lower thermal noise and reduced linear drift rate.

I. INTRODUCTION

Ultra-stable laser cavities are among the most precise measurement instruments currently in use, with applications spanning optical lattice clocks [1–4], gravitational wave detectors [5–7], and fundamental physics experiments [8–11]. The sensitivity of these systems is limited by various noise sources. In laser cavities, noise sources such as seismic vibrations, vacuum fluctuations, temperature instabilities, residual amplitude modulation, and parasitic etalons must also be carefully suppressed to achieve optimal system performance. These noise sources can often be minimized through careful engineering of the cavity system, including isolation systems, vacuum design, and optical and electronic components [12–16].

As a very important fundamental noise source, thermal noise of the cavity components currently limits the performance of ultra-stable laser cavities: mirror substrates, mirror coatings and the spacer [2, 17–19]. Over the years, numerous efforts have been made to mitigate thermal noise in order to enhance the performance. This has included using crystalline materials for mirror substrates [20, 21], improving the properties of the mirror coatings [22–26], exploring new coating materials [27–32], and lowering the system's temperature [2, 3]. Furthermore, reducing mirror thermal noise can also be achieved by manipulating the laser beam's spot size on the mirrors [33], using higher-order modes [34], or employing non-Gaussian beam shapes [35, 36].

Furthermore, the spacer contributes to the overall thermal noise budget. The spacer material is also crucial for

maintaining the distance between the mirrors and plays an essential role in ensuring long-term frequency stability, i.e., minimizing drift. To achieve both low thermal noise and minimized long-term drift, two well-studied spacer materials have been extensively used: Ultra-Low Expansion (ULE) glass from Corning Inc. and Zerodur® from Schott AG. These materials are favored for their extremely low coefficients of thermal expansion (CTE) around room temperature.

Recent interest has shifted toward NEXCERA™, a ceramic material from Krosaki Harima, due to its promising thermal and mechanical properties, which potentially offer superior performance in reducing both thermal noise and drift. NEXCERA's ultra-low thermal expansion around room temperature and high rigidity [37], with a Young's modulus of 140 GPa compared to ULE (67.6 GPa) and Zerodur (90.3 GPa), make it a strong candidate for next-generation spacer materials in ultra-stable laser cavities.

To assess NEXCERA's suitability for ultra-stable lasers, its mechanical loss factor must be determined to estimate the frequency stability when used as a spacer. The previously reported stability of NEXCERA based laser cavities reached a minimum Allan deviation (ADEV) of only $\sigma_y \approx 10^{-15}$ [38]. This is an order of magnitude bigger than predicted by the thermal floor dictated by dielectric coatings, which is the current main thermal limitation for ULE room-temperature cavities [2, 39].

NEXCERA N117B has demonstrated promising long-term stability, significantly reducing the effects of drift over time [38]. Minimizing long-term drift is crucial not only for metrological applications but also for fields like the search for Earth-like exoplanets [40, 41] and various fundamental physics experiments. These include

* These authors contributed equally to this work.

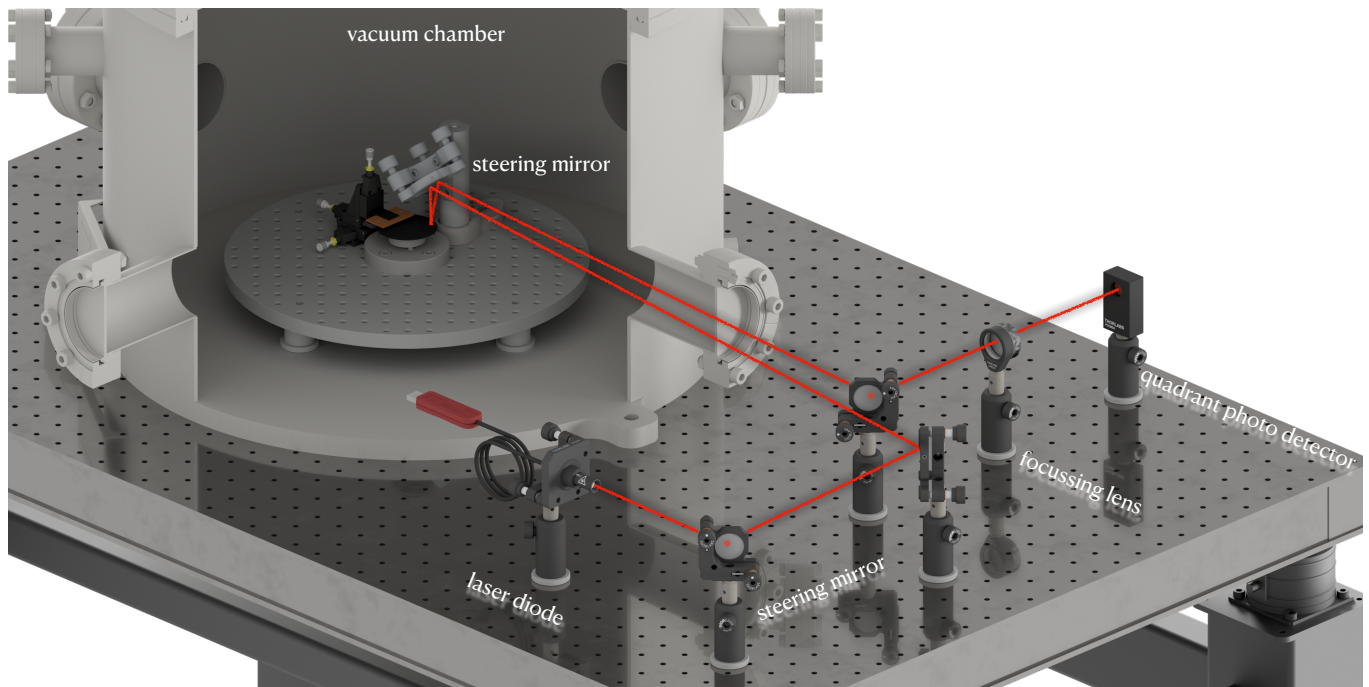


FIG. 1. Schematic of the Gentle Nodal Suspension setup on the optical table with an optical lever readout technique.

searches for dark matter [42], tests of Lorentz invariance violation [43, 44], constraints on quantum fluctuation amplitudes [43, 45], gravitational wave detection [46, 47], and searches for exotic particles beyond the Standard Model [47, 48].

The article is organized as follows: in the first section, we present the first ever reported mechanical losses of NEXCERA N117B. Here, the mechanical loss factor is analyzed across various resonance frequencies. The measurements are conducted at room temperature, as NEXCERA exhibits zero CTE at room temperature rendering it particularly appealing for room temperature applications [37].

In the second section, we present the predicted noise performance of the NEXCERA N117B cavity. Using our measured loss angle values, we calculate the Brownian thermal noise for the NEXCERA N117B spacer based on the fluctuation-dissipation theorem [49, 50], and compare it to commonly used room-temperature spacer materials. We also propose a cavity design with a NEXCERA N117B spacer and Fused Silica (FS) substrate, rather than the previously used ULE, to enhance the overall thermal performance of the ultra-stable optical cavity.

II. MECHANICAL LOSS FACTOR OF NEXCERA

Mechanical loss measurements are commonly performed by exciting a sample of the material to a mechanical resonance and measuring its ringdown time or the spectral linewidth of the resonance. Particularly

for ultra-low mechanical loss materials, such measurements often face significant systematic errors due to excess losses from the suspension mechanism holding the sample. These errors are particularly pronounced at temperatures around room temperature. Therefore, careful consideration and mitigation strategies are crucial to accurately access the intrinsic mechanical losses, which are key to determining the material's Brownian noise performance.

For this purpose, Cesarini *et al.* [51] developed the Gentle Nodal Suspension (GeNS) technique. The principle part of this technique is, that the sample is suspended at a single point, holding it in a stable equilibrium due to the gravitational force.

In this section, we investigate three NEXCERA disks made from the specific type N117B. All disks are geometrically identical, with a diameter of 50 mm, a thickness of 0.5 mm, and a surface roughness of ≤ 5 nm.

A. Experimental setup

The setup for the mechanical loss measurements is shown in Fig. 1. A 635 nm laser diode enables the optical readout of the sample oscillation. The laser beam is directed onto the sample's surface via a mirror, and the reflected beam exits the vacuum chamber at a slightly different angle. A steering mirror and lens then focus the beam onto the center of a quadrant photodetector, allowing for the detection of the sample's motion. As the sample oscillates at a resonant frequency, the reflected beam provides information on both the oscillation fre-

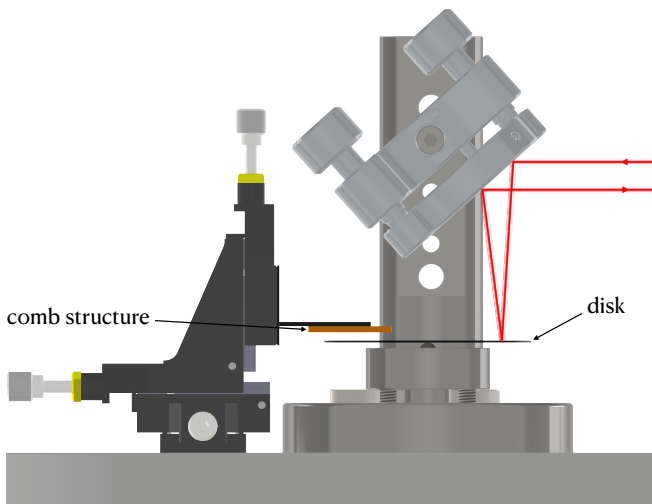


FIG. 2. Side view of the nodal support setup. The sample is suspended on a 4.5 mm steel ball clamped from a conical holding structure. The comb structure is used to excite the sample with a high voltage amplifier and can be positioned with a XYZ stage.

quency and amplitude. The signal from the quadrant detector is further used to calculate the mechanical loss factor.

To suppress residual gas damping which would impair the measured mechanical loss factor, we use a two-step pumping process. A rotary vane vacuum pump is connected to the vacuum chamber for preliminary vacuum pumping, where a turbomolecular pump is directly mounted on top of the vacuum cap. With this setup we achieve a vacuum pressure of 10^{-7} mbar. As the vacuum pump rotates at several tens of thousands of revolutions per minute, the resulting frequency is so high that it is effectively damped by the mass of the vacuum chamber.

A detailed view of the nodal suspension is shown in Fig. 2. We developed a custom sample holder based on the design by Cesarini *et al.* [51, 52], where a 4.5 mm steel ball is clamped from a conical head structure, protruding approximately 1 mm from the surface. The stability of the disk's suspension depends on both its geometry and the spherical suspension. If D is the diameter of the spherical suspension and t is the thickness of the disk, stable equilibrium is achieved when $D > t$ [51, 53]. For the stability condition, the potential energy V as a function of θ can be described by

$$V(\theta) = mg \left(\frac{D}{2} \cos \theta + \frac{D\theta}{2} \sin \theta + \frac{t}{2} \cos \theta \right), \quad (1)$$

where θ represents the angular position of the disk relative to the horizontal plane. The first term accounts for the vertical displacement of the disk's center from its initial position. The second term describes the height change due to the rotation induced by the tilted disk, while the third term denotes the alteration in height caused by the tilt itself.

Following this equation, the angular range conducive to stable oscillations can be derived as [51, 53]

$$\theta \lesssim \pm \sqrt{3} \frac{D-t}{t}. \quad (2)$$

Considering our specific geometries, the stability region is approximately $\theta \lesssim \pm 17^\circ$, which significantly exceeds the amplitude of the sample's oscillations.

As noted by Cesarini *et al.* [51], the suspension point influences the mechanical loss factor even though the variation is relatively small. In our efforts to minimize mechanical loss, we employed a strategy of adjusting the suspension point based on the following principle: Utilizing a 45° mirror positioned above the disk to direct the beam onto the sample, we leveraged the reflected beam to determine the relative displacement, thereby establishing an optical lever arm. By relocating the suspension point to a new equilibrium position, we could compare the relative displacement to the original laser spot, enabling us to estimate the disk's displacement within the micrometer range.

The contact area between the disk and the spherical suspension can be determined using Hertz's theory of surface contact [54]. According to this theory, when an elastic sphere with radius R indents an elastic half-space, the resulting contact area a , due to the applied force, is given by the following equation:

$$a = \left(\frac{3FR}{4E^*} \right)^{1/3}. \quad (3)$$

Here, $F = mg$ is the gravitational force applied to the disk, and E^* denotes the effective Young's modulus, which is defined as

$$\frac{1}{E^*} = \frac{1 - \sigma_{\text{sphere}}^2}{E_{\text{sphere}}} + \frac{1 - \sigma_{\text{sample}}^2}{E_{\text{sample}}}. \quad (4)$$

In this equation, σ and E represent the corresponding Poisson's ratios and Young's moduli.

In our configuration using the 4.5 mm sphere, the contact area of radius is approximately $10 \mu\text{m}$. Consequently, the suspension losses can be neglected for all modes in which the deformation at the center of the disk is nearly zero [53].

Furthermore, to mitigate the impact of surface roughness and defects caused by the suspended sphere, we utilize steel balls with a quality class of G3 according to DIN 5401 standards. This class offers the highest level of dimensional and shape accuracy.

The excitation of the disk is achieved through a comb structure, as illustrated in Fig. 2, which is controlled by a custom-built high-voltage amplifier. Positioned approximately 2 mm above the sample, the structure applies an oscillating voltage up to 800 V to drive the disk into its eigenmodes.

The force exerted can be derived from the energy stored between the comb structure and the disk,

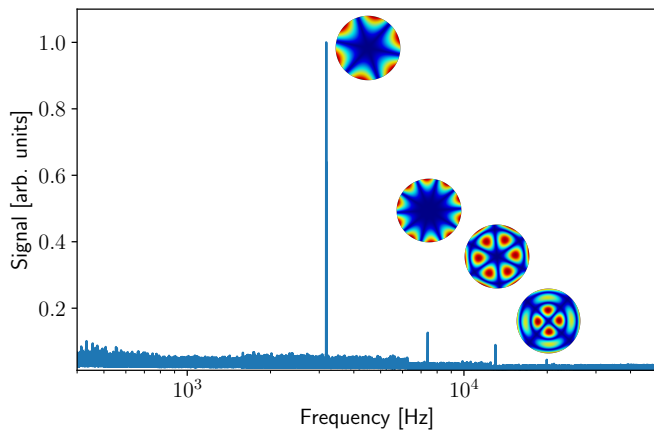


FIG. 3. Frequency spectrum from 500 Hz to 50 kHz with the corresponding mode pattern simulated with COMSOL. Four different mechanical modes can be observed, which are used for further loss investigations.

which is given by $E_C = CU^2/2$. From the relationship $F = -\partial E_C/\partial x$, the resulting force is harmonic and can be expressed as [55]

$$F = -\frac{1}{4} \frac{dC}{dx} \hat{U}^2 (1 - \cos 2\omega t). \quad (5)$$

Here, C represents the capacity between the plates, \hat{U} denotes the peak amplitude of the voltage, and ω is the angular frequency. Consequently, the sample is excited at twice its fundamental frequency, prompting the frequency generator to operate at half the resonant frequency.

B. Measurement results

To identify the eigenmodes of the sample, we present in Fig. 3 a frequency spectrum, where the frequency is scanned from 500 Hz to 50 kHz. We can identify four different resonance modes with the corresponding shapes of the oscillation, confirmed by finite element simulation based performed with COMSOL Multiphysics. The frequencies of the modes are $f_1 = 3.179$ kHz, $f_2 = 7.397$ kHz, $f_3 = 12.99$ kHz, and $f_4 = 21.16$ kHz.

The frequency spectrum in Fig. 3 shows narrow peaks, indicating a high quality factor. However, a mechanical ringdown to determine the decay time—and thus the mechanical loss factor—could not be performed. It appears that NEXCERA N117B exhibits material properties that cause it to be attracted to the comb structure during excitation. Since the excitation must be turned off to measure the decaying oscillation amplitude, the slight shift of the disk back to its original equilibrium disrupts the ringdown signal. As a result, we determine the loss angle from the resonance shape, fitting the experimental data to a Lorentzian function, as shown in Fig. 4. The loss

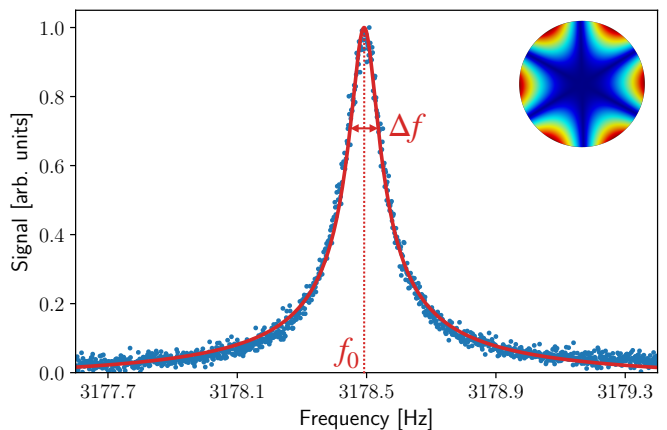


FIG. 4. Exemplary scan of a resonance for the fundamental mode. The bandwidth Δf and resonance frequency f_0 are used to determine the mechanical loss factor ϕ .

factor can be determined as

$$\phi = \frac{\Delta f}{f_0}, \quad (6)$$

where Δf is the bandwidth in which the signal amplitude drops to a factor of $1/\sqrt{2}$ and f_0 is the resonance frequency.

With these four mechanical resonances, we investigate the frequency-dependent mechanical loss factor for all three samples, presented in Fig. 5. Only a slight variation in the loss angle between the different disks and resonances can be observed. For disk 3, the lowest mechanical loss angle of $\phi = 1.894(41) \times 10^{-5}$ is measured.

Mechanical losses at room temperature are often limited by thermoelastic damping (TED) [56]. Each oscillation period of the mechanical vibration leads to a deformation, where certain areas are stretched and compressed, leading to an irreversible heat flux from the compressed (higher temperature) to the stretched part (lower temperature) [57]. However, due to the low CTE of NEXCERA N117B [37], TED should not be a limiting factor. Nevertheless, this loss mechanism should be studied to verify that it is not limiting the intrinsic energy dissipation.

Basically, the mechanical loss factor $\phi = \Delta E/(2\pi E)$ of a system is dependent on the ratio of the total energy E to the dissipated energy ΔE per oscillation period [57]. An entropy rise that causes an energy loss per cycle, derived from the heat equation, can be used to calculate the TED [58, 59]. The heat equation for a fully anisotropic treatment can be expressed as [60]

$$c_p \dot{T} - \kappa_{ij} \frac{\partial^2 T}{\partial x_i \partial x_j} = -\alpha_{ij} \dot{\sigma}_{ij} T_0, \quad (7)$$

where c_p is the specific heat per unit volume, and κ_{ij} is the tensor of thermal conductivity on the left-hand side. On the right-hand side, α_{ij} denotes the tensor CTE, σ_{ij} denotes the stress tensor, and T_0 denotes the average

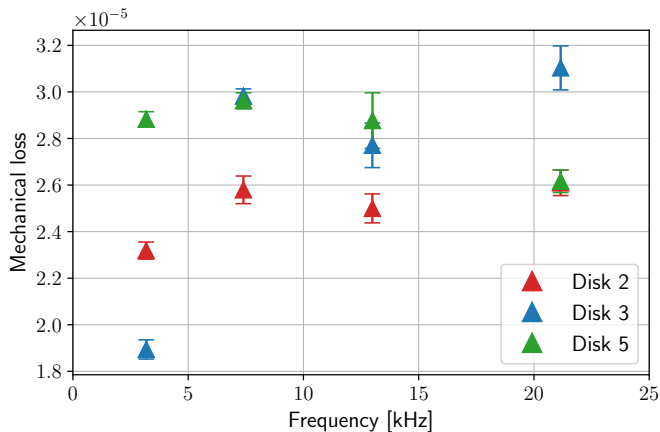


FIG. 5. Mechanical loss results for all three investigated samples and four different resonances. The lowest measured loss angle is $\phi = 1.894(41) \times 10^{-5}$ at $f_0 = 3.2$ kHz.

TABLE I. Material parameters used for TED simulation.

Parameter	Value
Young's modulus E	140 GPa [37]
Poisson's ratio σ	0.31 [37]
Coeff. of thermal expansion α	$0.03 \times 10^{-6}/\text{K}$ [37]
Thermal conductivity κ	4.2 W/(m K) [37]
Specific heat capacity c_p	780 J/(kg K) [37]
Mass density ρ	2550 kg/m ³ [37]

temperature of the sample. Solving this heat equation via finite element method, the dissipated energy can be calculated as [61]

$$\Delta E = \pi \int_V \alpha_{ij} \hat{\sigma}_{ij} \Im(\hat{T}) dV. \quad (8)$$

where $\Im(\hat{T})$ is the imaginary part of the resulting complex temperature field $\hat{T} = |\hat{T}|e^{i\omega t}$. Thus, the quality factor and therefore the mechanical loss can be calculated using Eq. (8) with the material properties given in Tab. I. In addition, the total energy E can also be derived from the simulation.

The COMSOL simulation gives the TED losses for the different vibrational modes as $\phi_{\text{TED},1} = 1.18 \times 10^{-10}$, $\phi_{\text{TED},2} = 2.93 \times 10^{-11}$, $\phi_{\text{TED},3} = 2.30 \times 10^{-11}$, and $\phi_{\text{TED},4} = 1.27 \times 10^{-11}$, respectively. Consequently, the TED is several orders of magnitude lower than the measured losses and is not a limiting factor at room temperature.

III. PERFORMANCE PROJECTION OF THE NEXCERA CAVITY

In the following sections, we present the projected performance of NEXCERA as a cavity spacer material and compare it to other common spacers. Key parameters

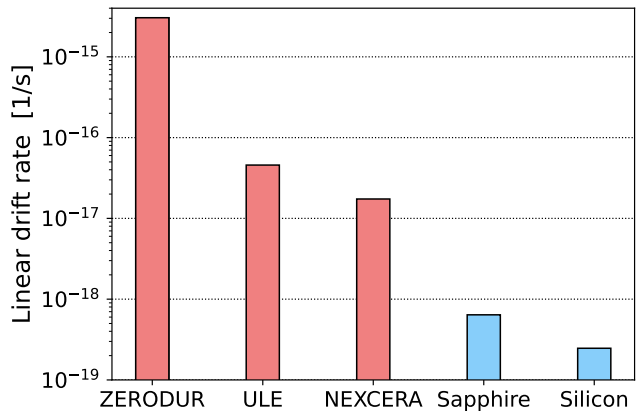


FIG. 6. Drift rate (1/s) for the most common materials used for the ultra-stable optical resonator spacers. ZERODUR [62], ULE [62] and NEXCERA N117B [38] operate at room temperature, whereas the single-crystal Silicon [4] and Sapphire [63] are used in a cryogenic environment. It is important to note that ULE drift rates vary significantly, with reported values ranging from $2.041 \times 10^{-16}/\text{s}$ [64] to $4.572 \times 10^{-17}/\text{s}$ [62]. This variation may be due to differences in measurement duration, environmental conditions, and specific glass samples.

evaluated include drift and Brownian thermal noise. Additionally, we discuss the noise improvement in NEXCERA cavities using FS mirror substrates compared to previously used ULE substrates.

A. Drift rate

Common spacer materials used at room temperature experience significant frequency drifts due to the crystallization of their amorphous structures. This ageing process causes the length of a Fabry-Perot spacer made of ULE, Zerodur, NEXCERA, or similar glass-ceramics to decrease, resulting in a positive drift in resonance frequency. Figure 6 compares the frequency drift rates of commonly used spacer materials. These are divided into amorphous materials at room temperature (red bars) and crystalline materials at cryogenic temperatures (blue bars). Both, ULE and NEXCERA exhibit drift rates two orders of magnitude lower than Zerodur, with NEXCERA N117B having a drift rate of $1.738 \times 10^{-17}/\text{s}$ compared to the best-reported value for ULE at $4.572 \times 10^{-17}/\text{s}$ [62]. Ageing processes slow over time [65, 66]. A decreasing drift rate with time indicates that older materials may perform better. The drift rates of NEXCERA and ULE spacers will reach the cavity thermal noise limit within a few seconds.

According to Fig. 6, drift can be suppressed using crystalline materials, such as single-crystal Silicon or Sapphire, which have nearly two orders of magnitude lower drift than NEXCERA. However, both Silicon [67, 68] and Sapphire [69, 70] have 2 to 3 orders of magnitude higher

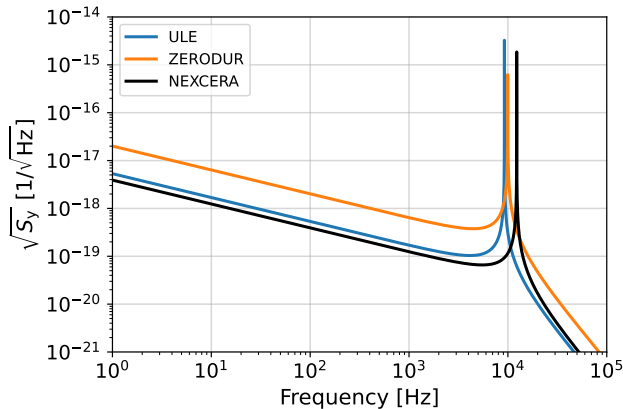


FIG. 7. Calculation of the fractional amplitude spectral density $\sqrt{S_y(f)}$ of the 30 cm long spacer made of Zerodur, ULE and measured in this work NEXCERA N117B.

CTE compared to ULE or NEXCERA, which significantly increases their sensitivity to temperature changes. This restricts the operational temperature of Silicon to the zero-crossing at 124 K and 16 K–17 K [71]. Furthermore, since the CTE tends towards zero as the temperature approaches 0 K, Sapphire and Silicon cavities often operate at ultra-low temperatures such as ~ 4 K [3, 72], ~ 1.5 K [71, 73, 74], or even in the sub-Kelvin regime [75]. Despite their crystalline structure being less prone to aging effects, in practice, Silicon and Sapphire also show a small long-term drift [68, 76].

This comparison illustrates, that NEXCERA is a promising material candidate for cavity spacers for room temperature applications provided that the thermal noise is sufficiently low.

B. Spacer Thermal Noise

The measurement data presented in this work allow us to recalculate the Brownian thermal noise for a spacer made of NEXCERA. Figure 7 illustrates the fractional amplitude spectral density $\sqrt{S_y(f)}$ of the Brownian noise for a 30 cm long spacer made of ULE, Zerodur, and NEXCERA. Brownian noise is calculated using the fluctuation-dissipation theorem [49, 50], in which the energy dissipation is linked to the measured loss angle ϕ [77]. A second type of fundamental temperature-related noise is known as thermoelastic noise [78, 79] depending mainly on the CTE. For the spacer materials presented in Fig. 7, the CTE is in the order of $\sim 10^{-9}$, see Tab. I, which makes thermoelastic noise negligible compared to the Brownian thermal noise.

In Fig. 7 the resonance frequencies f_0 of each material were determined analytically using $f_0 = (2L)^{-1}\sqrt{E/\rho}$, where L , E , and ρ represent the length, Young's modulus, and density of the spacer, respectively. Parameters used for the calculation of the resonance and Brownian

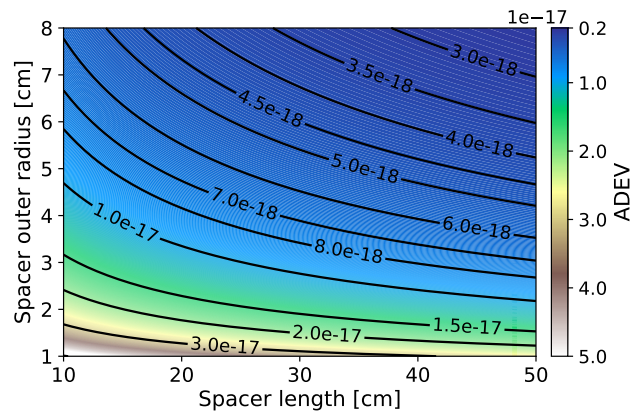


FIG. 8. The projected ADEV limit of the NEXCERA spacer in a function of spacer length and spacer outer radius. The inner bore radius is fixed to 6.35 mm, as in Refs. [2, 19].

thermal noise are presented in Tab. II. In general, the loss angle for thin structures have a larger value than for bulk materials like substrates and spacers, according to the surface-to-volume ratio and show also an increase of the loss for larger surface roughnesses and higher structural impurity densities [56, 80–82]. Therefore, best-measured values of the NEXCERA thin discs are still conservative estimations of the loss angle value for the bulk bodies such as the spacer.

Figure 7 shows that the Brownian noise performance of NEXCERA is superior to that of ULE and Zerodur at frequencies below the resonance. At frequencies above the resonance frequency, the noise of NEXCERA is slightly higher than that of ULE but still lower than that of Zerodur. Moreover, the resonance frequency of NEXCERA is higher than that of ULE and Zerodur, indicating that the designed bandwidth of the cavity is greater.

The long-term instability of ultra-stable cavities is typically represented in the time domain by the ADEV [19, 38]. The ADEV of the Brownian noise is given by a constant value and can be recalculated from the power spectral density as follows: $\sigma_y = \sqrt{2\ln(2)S_y f}$ [83]. Figure 8 illustrates the Brownian thermal noise limit for the NEXCERA spacer in the shape of a hollow cylinder as a function of spacer length and outer radius. The inner bore radius is fixed at 6.35 mm [2, 19]. As the outer radius (and consequently the mass) increases, the thermal noise floor decreases.

These calculated values of the ADEV are several orders of magnitude lower for all spacer lengths and outer radii shown compared to the best previously reported NEXCERA cavity, which has a minimum ADEV of 10^{-15} [38]. Thus, the dominant noise contribution is not limited by the Brownian thermal noise of the NEXCERA spacer and further designs of cavities show a low enough noise compared to the most-stable room-temperature cavity [19].

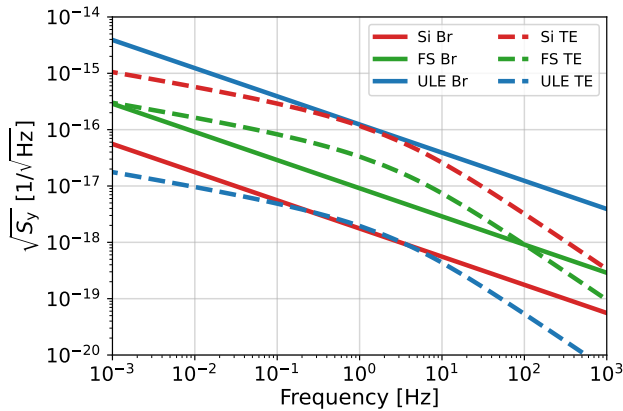


FIG. 9. Brownian (Br) and thermoelastic (TE) noises shown as fractional amplitude spectral density $\sqrt{S_y(f)}$ for the three types of the substrates: ULE, FS and Si. The spacers are 30 cm long, and the mirrors are plano-concave with ROC of 1 m.

TABLE II. Spacer material constants, such as Young modulus E , mass density ρ , Poisson's ratio σ , and the loss angle ϕ in 293 K used for the calculations of the spacer Brownian thermal noise.

Material	E [GPa]	ρ [kg/m ³]	σ	ϕ [10 ⁻⁵]
Zerodur	90.3 [84]	2530 [84]	0.24 [84]	32 [17]
ULE	67.6 [85]	2210 [85]	0.17 [85]	1.6 [17]
NEXCERA	140 [37]	2550 [37]	0.31 [37]	1.9 [this work]

C. Noise Performance of NEXCERA Spacers with Fused Silica Mirror Substrates

The best room-temperature optical resonators are currently made of ULE spacer and FS substrates [2, 19]. FS has even two orders of magnitude [86] smaller loss angle than ULE [17], resulting in overall better cavity performance, compared to the one with ULE substrates.

So far, all reported NEXCERA ultra-stable cavities have been equipped with ULE substrates [38, 87, 88]. Both materials have similar CTE and zero-crossing points [87], which effectively does not shift the combined NEXCERA-ULE zero-crossing point. In this section, we propose to replace ULE with FS. Combining different materials with mismatched CTE's can be handled, using carefully designed compensation rings [16].

Figure 9 shows the Brownian and thermoelastic noise generated by ULE, FS, and Silicon (Si) mirror substrates. Because of the small CTE, ULE's thermoelastic noise is negligible, but the high loss angle and, therefore, high Brownian noise dominates the substrate's overall performance. Si has the lowest Brownian but the highest thermoelastic noise. An optimal choice, i.e. smallest uncorrelated sum of Brownian and thermoelastic noise for room-temperature cavities, is FS substrates.

Figure 10 illustrates the overall NEXCERA spacer cavity noise with crystalline coatings [28] and three substrate

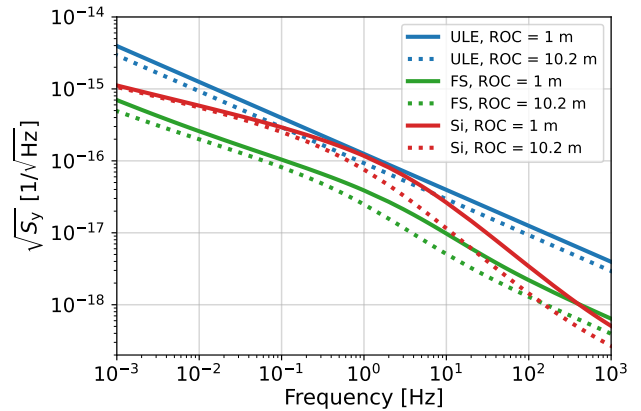


FIG. 10. Total $\sqrt{S_y(f)}$ of a NEXCERA spacer cavity for three possible substrates materials with crystalline coatings and two ROC (1 m and 10.2 m) of plano-concave configuration.

configurations. Since both Brownian and thermoelastic noise depends on the beam spot size on the mirrors, two radii of curvature (ROC) are presented: the commonly used ROC of 1 m [19] and the 10.2 m ROC, which is the largest commercially available for high-finesse performance. Replacing ULE with FS improves the performance of the cavity across the entire frequency range: at 1 Hz, the improvement for the ROC of 10.2 m is a factor of 4.

IV. CONCLUSION

This work presents the first mechanical loss data for NEXCERA N117B. We achieved a lowest mechanical loss of $\phi = 1.89 \times 10^{-5}$, which is significantly lower than that of Zerodur ($\phi = 3.2 \times 10^{-4}$) and very similar to that of ULE ($\phi = 1.6 \times 10^{-5}$). Using our measured data, we calculate the theoretical cavity performance with respect to Brownian thermal noise and compare it to ULE and Zerodur. In addition, we discussed the drift of these materials as cavity spacers and the influence of different mirror substrate materials on the noise performance. Our results underline that NEXCERA is a highly appealing material for cavity spacers in ultra-stable laser interferometers, as its calculated Brownian thermal noise is lower than that of ULE and Zerodur, making it more sensitive to measuring low-frequency signals, such as gravitational waves. Furthermore, its higher rigidity suggests that larger NEXCERA cavities may be less sensitive to vibrations, potentially simplifying their mechanical support.

ACKNOWLEDGMENT

The authors thank J. Dickmann for technical support. This project (20FUN08 NEXTLASERS) has received funding from the EMPIR programme co-financed by

the Participating States and from the European Union's Horizon 2020 research and innovation programme, and by the Deutsche Forschungsgemeinschaft (DFG, German Research Foundation) under Germany's Excellence Strategy–EXC-2123 QuantumFrontiers–390837967.

-
- [1] A. D. Ludlow, M. M. Boyd, J. Ye, E. Peik, and P. O. Schmidt, Optical atomic clocks, *Rev. Mod. Phys.* **87**, 637 (2015).
- [2] D. G. Matei *et al.*, 1.5 μm Lasers with Sub-10 mHz Linewidth, *Phys. Rev. Lett.* **118**, 263202 (2017).
- [3] W. Zhang *et al.*, Ultrastable Silicon Cavity in a Continuously Operating Closed-Cycle Cryostat at 4 K, *Phys. Rev. Lett.* **119**, 243601 (2017).
- [4] E. Oelker *et al.*, Demonstration of 4.8×10^{-17} stability at 1 s for two independent optical clocks, *Nat. Photon.* **13**, 714 (2019).
- [5] Y. Aso, Y. Michimura, K. Somiya, M. Ando, O. Miyakawa, T. Sekiguchi, D. Tatsumi, and H. Yamamoto (The KAGRA Collaboration), Interferometer design of the KAGRA gravitational wave detector, *Phys. Rev. D* **88**, 043007 (2013).
- [6] B. P. Abbott *et al.*, Observation of gravitational waves from a binary black hole merger, *Phys. Rev. Lett.* **116**, 061102 (2016).
- [7] B. Sathyaprakash *et al.*, Scientific objectives of Einstein Telescope, *Class. Quantum Grav.* **29**, 124013 (2012).
- [8] A. P. Higginbotham, P. S. Burns, M. D. Urmey, R. W. PETERSON, N. S. Kampel, B. M. Brubaker, G. Smith, K. W. Lehnert, and C. A. Regal, Harnessing electro-optic correlations in an efficient mechanical converter, *Nat. Phys.* **14**, 1038 (2018).
- [9] G. Marra *et al.*, Ultrastable laser interferometry for earthquake detection with terrestrial and submarine cables, *Science* **361**, 486 (2018).
- [10] W. R. Milner *et al.*, Demonstration of a Timescale Based on a Stable Optical Carrier, *Phys. Rev. Lett.* **123**, 173201 (2019).
- [11] C. J. Kennedy, E. Oelker, J. M. Robinson, T. Bothwell, D. Kedar, W. R. Milner, G. E. Marti, A. Derevianko, and J. Ye, Precision Metrology Meets Cosmology: Improved Constraints on Ultralight Dark Matter from Atom-Cavity Frequency Comparisons, *Phys. Rev. Lett.* **125**, 201302 (2020).
- [12] T. Nazarova, F. Riehle, and U. Sterr, Vibration-insensitive reference cavity for an ultra-narrow-linewidth laser, *Appl. Phys. B* **83**, 531 (2006).
- [13] L. Chen, J. L. Hall, J. Ye, T. Yang, E. Zang, and T. Li, Vibration-induced elastic deformation of fabry-perot cavities, *Phys. Rev. A* **74**, 053801 (2006).
- [14] S. Braccini *et al.*, Measurement of the seismic attenuation performance of the VIRGO Superattenuator, *Astropart. Phys.* **23**, 557 (2005).
- [15] F. Riehle, *Frequency Standards* (John Wiley & Sons, Ltd, 2003).
- [16] T. Legero, T. Kessler, and U. Sterr, Tuning the thermal expansion properties of optical reference cavities with fused silica mirrors, *J. Opt. Soc. Am. B* **27**, 914 (2010).
- [17] K. Numata, A. Kemery, and J. Camp, Thermal-noise limit in the frequency stabilization of lasers with rigid cavities, *Phys. Rev. Lett.* **93**, 250602 (2004).
- [18] T. Kessler, C. Hagemann, C. Grebing, T. Legero, U. Sterr, F. Riehle, M. Martin, L. Chen, and J. Ye, A sub-40-mHz-linewidth laser based on a silicon single-crystal optical cavity, *Nat. Photon.* **6**, 687 (2012).
- [19] S. Häfner, S. Falke, C. Grebing, S. Vogt, T. Legero, M. Merimaa, C. Lisdat, and U. Sterr, 8×10^{-17} fractional laser frequency instability with a long room-temperature cavity, *Opt. Lett.* **40**, 2112 (2015).
- [20] R. Nawrodt, A. Zimmer, T. Koettig, S. Nietzsche, M. Thürk, W. Vodel, and P. Seidel, High mechanical Q-factor measurements on calcium fluoride at cryogenic temperatures, *Eur. Phys. J. Appl. Phys.* **38**, 53 (2007).
- [21] R. Nawrodt, A. Zimmer, T. Koettig, C. Schwarz, D. Heinert, M. Hudl, R. Neubert, M. Thürk, S. Nietzsche, W. Vodel, P. Seidel, and A. Tünnermann, High mechanical Q-factor measurements on silicon bulk samples, *J. Phys.: Conf. Ser.* **122**, 012008 (2008).
- [22] S. D. Penn *et al.*, Mechanical loss in tantala/silica dielectric mirror coatings, *Class. Quantum Grav.* **20**, 2917 (2003).
- [23] I. W. Martin *et al.*, Effect of heat treatment on mechanical dissipation in Ta_2O_5 coatings, *Class. Quantum Grav.* **27**, 225020 (2010).
- [24] I. Martin *et al.*, Measurements of a low-temperature mechanical dissipation peak in a single layer of Ta_2O_5 doped with TiO_2 , *Class. Quantum Grav.* **25**, 055005 (2008).
- [25] G. M. Harry *et al.*, Titania-doped tantala/silica coatings for gravitational-wave detection, *Class. Quantum Grav.* **24**, 405 (2006).
- [26] M. Granata *et al.*, Amorphous optical coatings of present gravitational-wave interferometers*, *Class. Quantum Grav.* **37**, 095004 (2020).
- [27] D. R. M. Crooks *et al.*, Experimental measurements of mechanical dissipation associated with dielectric coatings formed using SiO_2 , Ta_2O_5 and Al_2O_3 , *Class. Quantum Grav.* **23**, 4953 (2006).
- [28] G. D. Cole, W. Zhang, M. J. Martin, J. Ye, and M. Aspelmeyer, Tenfold reduction of brownian noise in high-reflectivity optical coatings, *Nat. Photon.* **7**, 644 (2013).
- [29] G. Vajente *et al.*, Low Mechanical Loss $\text{TiO}_2\text{:GeO}_2$ Coatings for Reduced Thermal Noise in Gravitational Wave Interferometers, *Phys. Rev. Lett.* **127**, 071101 (2021).
- [30] J. Dickmann and S. Kroker, Highly reflective low-noise etalon-based meta-mirror, *Phys. Rev. D* **98**, 082003 (2018).
- [31] G. I. McGhee *et al.*, Titania mixed with silica: A low thermal-noise coating material for gravitational-wave detectors, *Phys. Rev. Lett.* **131**, 171401 (2023).
- [32] J. Dickmann, S. Sauer, J. Meyer, M. Gaedtke, T. Siefke, U. Brückner, J. Plentz, and S. Kroker, Experimental realization of a 12,000-finesse laser cavity based on a low-noise microstructured mirror, *Commun. Phys.* **6**, 16 (2023).

- [33] S. Amairi, T. Legero, T. Kessler, U. Sterr, J. B. Wübbena, O. Mandel, and P. O. Schmidt, Reducing the effect of thermal noise in optical cavities, *Appl. Phys. B* **113**, 233 (2013).
- [34] J.-Y. Vinet, Thermal noise in advanced gravitational wave interferometric antennas: A comparison between arbitrary order hermite and laguerre gaussian modes, *Phys. Rev. D* **82**, 042003 (2010).
- [35] E. D’Ambrosio, Nonspherical mirrors to reduce thermoelastic noise in advanced gravitational wave interferometers, *Phys. Rev. D* **67**, 102004 (2003).
- [36] M. Bondarescu and K. S. Thorne, New family of light beams and mirror shapes for future ligo interferometers, *Phys. Rev. D* **74**, 082003 (2006).
- [37] T. Nose, M. Nakabayashi, N. Kosugi, F. Takahashi, and H. Morita, NEXCERA: Ultra low thermal expansion ceramics, Nippon Steel Technical Report **84** (2001).
- [38] I. Ito, A. Silva, T. Nakamura, and Y. Kobayashi, Stable CW laser based on low thermal expansion ceramic cavity with 4.9 mHz/s frequency drift, *Opt. Express* **25**, 26020 (2017).
- [39] J. M. Robinson *et al.*, Thermal noise and mechanical loss of SiO₂/Ta₂O₅ optical coatings at cryogenic temperatures, *Opt. Lett.* **46**, 592 (2021).
- [40] M. T. Murphy *et al.*, High-precision wavelength calibration of astronomical spectrographs with laser frequency combs, *Monthly Notices of the Royal Astronomical Society* **380**, 839 (2007).
- [41] T. Steinmetz *et al.*, Laser frequency combs for astronomical observations, *Science* **321**, 1335 (2008).
- [42] P. Wcisło *et al.*, New bounds on dark matter coupling from a global network of optical atomic clocks, *Sci. Adv.* **4**, eaau4869 (2018).
- [43] Q. Chen, E. Magoulakis, and S. Schiller, High-sensitivity crossed-resonator laser apparatus for improved tests of lorentz invariance and of space-time fluctuations, *Phys. Rev. D* **93**, 022003 (2016).
- [44] N. Gürlebeck *et al.*, BOOST: A satellite mission to test lorentz invariance using high-performance optical frequency references, *Phys. Rev. D* **97**, 124051 (2018).
- [45] S. Schiller, C. Lämmerzahl, H. Müller, C. Braxmaier, S. Herrmann, and A. Peters, Experimental limits for low-frequency space-time fluctuations from ultrastable optical resonators, *Phys. Rev. D* **69**, 027504 (2004).
- [46] S. Kolkowitz, I. Pikovski, N. Langellier, M. D. Lukin, R. L. Walsworth, and J. Ye, Gravitational wave detection with optical lattice atomic clocks, *Phys. Rev. D* **94**, 124043 (2016).
- [47] M. Narožnik, M. Bober, and M. Zawada, Ultra-stable optical clock cavities as resonant mass gravitational wave detectors in search for new physics, *Phys. Lett. B* **846**, 138260 (2023).
- [48] A. A. Geraci, C. Bradley, D. Gao, J. Weinstein, and A. Derevianko, Searching for ultralight dark matter with optical cavities, *Phys. Rev. Lett.* **123**, 031304 (2019).
- [49] H. B. Callen and T. A. Welton, Irreversibility and Generalized Noise, *Phys. Rev.* **83**, 34 (1951).
- [50] H. B. Callen and R. F. Greene, On a Theorem of Irreversible Thermodynamics, *Phys. Rev.* **86**, 702 (1952).
- [51] E. Cesarini, M. Lorenzini, E. Campagna, F. Martelli, F. Piergiovanni, F. Vetrano, G. Losurdo, and G. Cagnoli, A “gentle” nodal suspension for measurements of the acoustic attenuation in materials, *Rev. Sci. Instrum.* **80**, 053904 (2009).
- [52] E. Cesarini, M. Lorenzini, G. Cagnoli, and F. Piergiovanni, A gentle nodal suspension for measurements of the acoustic attenuation in materials, in *2014 IEEE Metrology for Aerospace (MetroAeroSpace)* (2014) pp. 528–532.
- [53] G. Vajente, A. Ananyeva, G. Billingsley, E. Gustafson, A. Heptonstall, E. Sanchez, and C. Torrie, A high throughput instrument to measure mechanical losses in thin film coatings, *Rev. Sci. Instrum.* **88**, 073901 (2017).
- [54] K. L. Johnson, *Contact Mechanics* (Cambridge University Press, 1985).
- [55] R. Nawrodt, *Kryogene Gütemessung an optischen Substratmaterialien für zukünftige Gravitationswellendetektoren*, Ph.D. thesis, Friedrich-Schiller-Universität Jena (2008).
- [56] R. Nawrodt *et al.*, Investigation of mechanical losses of thin silicon flexures at low temperatures, *Class. Quantum Grav.* **30**, 115008 (2013).
- [57] R. Lifshitz and M. L. Roukes, Thermoelastic damping in micro- and nanomechanical systems, *Phys. Rev. B* **61**, 5600 (1999).
- [58] M. M. Fejer, S. Rowan, G. Cagnoli, D. R. M. Crooks, A. Gretarsson, G. M. Harry, J. Hough, S. D. Penn, P. H. Sneddon, and S. P. Vyatchanin, Thermoelastic dissipation in inhomogeneous media: loss measurements and displacement noise in coated test masses for interferometric gravitational wave detectors, *Phys. Rev. D* **70**, 082003 (2004).
- [59] C. Cagnoli *et al.*, Mode-dependent mechanical losses in disc resonators, *Phys. Lett. A* **382**, 2165 (2018).
- [60] A. N. Norris and D. M. Photiadis, Thermoelastic relaxation in elastic structures, with applications to thin plates, *Q. J. Mech. Appl. Math.* **58**, 143 (2005).
- [61] D. Heinert *et al.*, Potential mechanical loss mechanisms in bulk materials for future gravitational wave detectors, *J. Phys.: Conf. Ser.* **228**, 012032 (2010).
- [62] J. Keupp, A. Douillet, T. E. Mehlstäubler, N. Rehbein, E. M. Rasel, and W. Ertmer, A high-resolution Ramsey-Bordé spectrometer for optical clocks based on cold Mg atoms, *Eur. Phys. J. D* **36**, 289 (2005).
- [63] E. Wiens, A. Y. Nevsky, and S. Schiller, Resonator with ultrahigh length stability as a probe for equivalence-principle-violating physics, *Phys. Rev. Lett.* **117**, 271102 (2016).
- [64] J. Alnis, A. Matveev, N. Kolachevsky, T. Udem, and T. W. Hänsch, Subhertz linewidth diode lasers by stabilization to vibrationally and thermally compensated ultralow-expansion glass Fabry-Pérot cavities, *Phys. Rev. A* **77**, 053809 (2008).
- [65] J. C. Phillips, Stretched exponential relaxation in molecular and electronic glasses, *Rep. Prog. Phys.* **59**, 1133 (1996).
- [66] P. Dubé, A. A. Madej, J. E. Bernard, L. Marmet, and A. D. Shiner, A narrow linewidth and frequency-stable probe laser source for the ⁸⁸Sr⁺ single ion optical frequency standard, *Appl. Phys. B* **95**, 43 (2009).
- [67] T. Middelmann, A. Walkov, G. Bartl, and R. Schödel, Thermal expansion coefficient of single-crystal silicon from 7 K to 293 K, *Phys. Rev. B* **92**, 174113 (2015).
- [68] E. Wiens, C. J. Kwong, T. Müller, and S. Schiller, A simplified cryogenic optical resonator apparatus providing ultra-low frequency drift, *Rev. Sci. Instrum.* **91**, 045112 (2020).
- [69] Y. S. Touloukian, R. K. Kirby, E. R. M. Taylor, and T. Y. R. Lee, in *Thermophysical Properties of Matter -*

- the TPRC Data Series. Volume 13. Thermal Expansion - Nonmetallic Solids* (1977).
- [70] C. Taylor, M. Notcutt, E. Wong, A. Mann, and D. Blair, Measurement of the coefficient of thermal expansion of a cryogenic, all-sapphire, Fabry-Perot optical cavity, *Opt. Commun.* **131**, 311 (1996).
- [71] E. Wiens, Q.-F. Chen, I. Ernsting, H. Luckmann, U. Rosowski, A. Nevsky, and S. Schiller, Silicon single-crystal cryogenic optical resonator, *Opt. Lett.* **39**, 3242 (2014).
- [72] H. Müller, S. Herrmann, C. Braxmaier, S. Schiller, and A. Peters, Modern Michelson-Morley Experiment using Cryogenic Optical Resonators, *Phys. Rev. Lett.* **91**, 020401 (2003).
- [73] S. Seel, R. Storz, G. Ruoso, J. Mlynek, and S. Schiller, Cryogenic Optical Resonators: A New Tool for Laser Frequency Stabilization at the 1 Hz Level, *Phys. Rev. Lett.* **78**, 4741 (1997).
- [74] E. Wiens, C. J. Kwong, T. Müller, K. Bongs, Y. Singh, and S. Schiller, Optical frequency reference based on a cryogenic silicon resonator, *Opt. Express* **31**, 42059 (2023).
- [75] J. Barbarat, J. Gillot, J. Millo, C. Lacroûte, V. Giordano, Y. Kersalé, and T. Legero, Development of a Sub-Kelvin Silicon Cavity, in *2023 Joint Conference of the European Frequency and Time Forum and IEEE International Frequency Control Symposium (EFTF/IFCS)* (2023) pp. 1–2.
- [76] J. G. Hartnett, C. R. Locke, E. N. Ivanov, M. E. Tobar, and P. L. Stanwix, Cryogenic sapphire oscillator with exceptionally high long-term frequency stability, *Appl. Phys. Lett.* **89**, 203513 (2006).
- [77] P. R. Saulson, Thermal noise in mechanical experiments, *Phys. Rev. D* **42**, 2437 (1990).
- [78] Y. T. Liu and K. S. Thorne, Thermoelastic noise and homogeneous thermal noise in finite sized gravitational-wave test masses, *Phys. Rev. D* **62**, 122002 (2000).
- [79] T. Chalermongsak, F. Seifert, E. D. Hall, K. Arai, E. K. Gustafson, and R. X. Adhikari, Broadband measurement of coating thermal noise in rigid Fabry–Pérot cavities, *Metrologia* **52**, 17 (2014).
- [80] A. M. Gretarsson and G. M. Harry, Dissipation of mechanical energy in fused silica fibers, *Rev. Sci. Instrum.* **70**, 4081 (1999).
- [81] A. Ageev, B. C. Palmer, A. D. Felice, S. D. Penn, and P. R. Saulson, Very high quality factor measured in annealed fused silica, *Class. Quantum Grav.* **21**, 3887 (2004).
- [82] S. D. Penn, A. Ageev, D. Busby, G. M. Harry, A. M. Gretarsson, K. Numata, and P. Willems, Frequency and surface dependence of the mechanical loss in fused silica, *Phys. Lett. A* **352**, 3 (2006).
- [83] T. Kessler, T. Legero, and U. Sterr, Thermal noise in optical cavities revisited, *J. Opt. Soc. Am. B* **29**, 178 (2012).
- [84] Advanced Optics SCHOTT AG, ZERODUR (2023), Accessed: 2024-09-17.
- [85] Corning Advanced Optics, Corning ULE 7973 Low Expansion Glass (2015), Accessed: 2024-09-17.
- [86] A. Schroeter *et al.*, On the mechanical quality factors of cryogenic test masses from fused silica and crystalline quartz, arXiv **0709.4359** (2007).
- [87] K. Hosaka, H. Inaba, D. Akamatsu, M. Yasuda, J. Sugawara, A. Onae, and F.-L. Hong, A Fabry–Pérot Etalon with an Ultralow Expansion Ceramic Spacer, *Jpn. J. Appl. Phys.* **52**, 032402 (2013).
- [88] C. J. Kwong, M. G. Hansen, J. Sugawara, and S. Schiller, Characterization of the long-term dimensional stability of a NEXCERA block using the optical resonator technique, *Meas. Sci. Technol.* **29**, 075011 (2018).